*Materials Transactions*, Vol. 64, No. 10 (2023) pp. 2425 to 2430
Special Issue on Metallurgy for Advanced Catalytic Materials


# Catalytic Properties and Their Relation with Adsorption Energies Calculated by Density Functional Theory in Pd-Containing 1/1 Approximant Crystals

Haruka Yoshikawa[1,2,*1], Farid Labib[1], Ya Xu[2,*2] and Ryuji Tamura[1]

[1]*Department of Materials Science and Technology, Tokyo University of Science, Tokyo 125-8585, Japan*
[2]*Center for Green Research on Energy and Environmental Materials, National Institute for Materials Science, Tsukuba 305-0003, Japan*

Quasicrystals and approximant crystals (ACs) have a unique complex structure with many crystallographically non-equivalent sites. In order to apply this characteristic potential to catalysts, we investigated catalytic properties of Pd-containing Tsai-type 1/1 ACs, i.e., Al–Pd–Sc and Ga–Pd–Sc, in the acetylene hydrogenation reaction and also performed density functional theory calculations of adsorption energies of reactants and products. The catalytic properties are found to significantly depend on the kind of the semimetal element such as Al and Ga, where the Al–Pd–Sc 1/1 AC shows higher catalytic activity and selectivity. The adsorption energy of reactant acetylene is smaller in the Al–Pd–Sc 1/1 AC whereas the amount of product ethylene are comparable for both ACs. Therefore, the adsorption rate of reactants is increased while the desorption rate of products remains almost the same in the Al–Pd–Sc 1/1 AC. Furthermore, the adsorption energies are found to differ significantly from site to site, implying a superior potential of ACs for designation of active sites using many non-equivalent crystallographic sites for high catalytic performance. [doi:10.2320/matertrans.MT-MH2022006]

(Received April 5, 2023; Accepted June 1, 2023; Published June 16, 2023)

**Keywords:** *catalyst, Tsai-type 1/1 approximant crystals, acetylene hydrogenation, density functional theory, catalytic activity, selectivity, non-equivalent crystallographic site*

## 1. Introduction

The ligand and ensemble effects are of significant importance for the improvement of the catalytic properties of metal catalysts.[1–4] These effects are related to the local structure of the surface and therefore are considered to be controllable by the atomic arrangement. However, it is highly challenging to design catalysts by manipulating the local structure at the atomic level even today. In this study, we attempt to design the local structure by using metallic compounds that have many crystallographically non-equivalent sites that can be substituted with other elements.

Typical examples of such materials are quasicrystals and approximant crystals (ACs), which are a group of materials composed of an icosahedral cluster made of concentric polyhedral atomic shells.[5,6] In quasicrystals, the icosahedral clusters are quasiperiodically arranged whereas they are periodically arranged in ACs. For example, in 1/1 ACs, the icosahedral clusters are arranged in a body centered cubic lattice. Due to the unique complex cluster structure, these materials have many non-equivalent crystallographic sites. Several studies on the catalytic properties of quasicrystals and related materials have been performed so far, and much attention has been paid to new catalysts originating from their unique structures.[7–16] In this work, materials composed of the Tsai-type cluster are chosen for the investigation of catalytic properties: The Tsai-type cluster is a type of icosahedral cluster where rare earth elements occupy the vertices of the inner icosahedron shell among various concentric shells, and many compounds composed of the Tsai-type cluster have been discovered in recent years.[17]

The objective of this study is to evaluate the catalytic properties of Pd-containing Al–Pd–Sc and Ga–Pd–Sc compounds, which are classified as Tsai-type 1/1 ACs.[18,19] and to investigate the relationship between the characteristic structure and catalytic properties by calculating adsorption energies using density functional theory (DFT). For this purpose, the $C_2H_2$ hydrogenation reaction (eq. (1)) was chosen since the reaction can be performed at relatively low temperatures even with bulk metal and hence sample degradation during the reaction is suppressed due to the absence of oxygen, and, furthermore, the mechanism of ethylene hydrogenation as a side reaction is simple, making it easy to evaluate the selectivity of the catalyst.[20]

$$C_2H_2 + H_2 \rightarrow C_2H_4 \quad \Delta H = -173\,\mathrm{kJ/mol}\ (298\,\mathrm{K}) \quad (1)$$

## 2. Experimental Procedure

### 2.1 Sample preparation

Ingots weighing approximately 0.7 g of polycrystalline 1/1 ACs with nominal compositions of $Ga_{55}Pd_{30}Sc_{15}$ and $Al_{55}Pd_{30}Sc_{15}$ were prepared from highly pure elements using arc-melting technique under Ar atmosphere. The alloy ingots were crushed to powder with a particle size of 75 μm or less under argon atmosphere as catalysts sample. The amount of power catalyst for reaction was approximately 0.1 g.

### 2.2 Sample characterization

For phase identification, X-Ray diffraction (XRD) measurement was carried out using Rigaku SmartLab SE and Rigaku MiniFlex600 diffractometers with Cu K$\alpha$.

The Brunauer–Emmett–Teller (BET) specific surface areas measurement of the crushed powder samples were performed using specific-surface-area analyzer (Micrometrics, ASAP2020). Since the metal powder has a small surface area, Kr was used as the adsorption gas.

### 2.3 Catalytic performance

The $C_2H_2$ hydrogenation reaction test was conducted in a fixed-bed flow reactor. The catalyst powder sample was

*1Graduate Student, Tokyo University of Science
*2Corresponding author, E-mail: XU.Ya@nims.go.jp

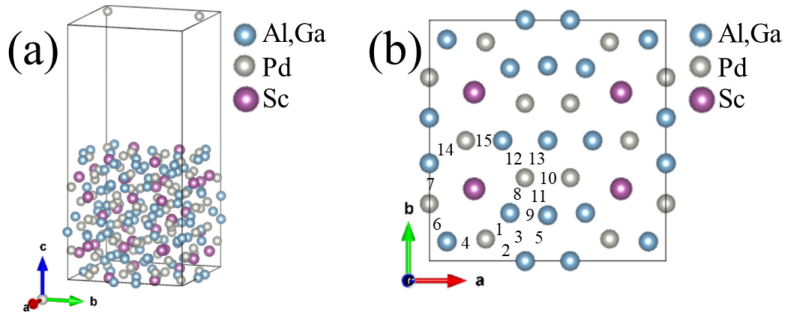


Fig. 1 (a) Al–Pd–Sc and Ga–Pd–Sc 1/1 ACs (100) slab structure model based on the results of HAADF-STEM structure analysis.[21,22] (b) Surface layer of the slab and adsorption points on the bridge site from 1 to 15.

loaded into quartz reaction tube with an inner diameter of 8 mm and thermocouple inserted just beneath the sample to control sample temperature. Prior to the reaction, the sample was reduced under hydrogen flow (30.0 mL/min) at 430°C for 1 h. The reaction gas was supplied from a mixture gas (2.19 vol% $C_2H_2$–$N_2$) cylinder and a pure hydrogen gas cylinder, the feed composition of $C_2H_2$, hydrogen, and $N_2$, were 0.5, 5.0, and 23.8 mL/min, respectively. The reaction was performed by increasing the temperature from 120 to 200°C at 20°C intervals, and the incubation time for each temperature was 30 minutes. The composition of the products obtained during the reaction was analyzed several times at each temperature using a online gas chromatography system (GL Science, GC323, GL Science, GC-4000 Plus). A zeolite adsorbent column (13X molecular sieve) was used to separate $H_2$ and $N_2$. A DVB-EVB-Ethyleneglycol dimethacrylate column (Polapak N 80/100) was used to separate $C_2H_2$, $C_2H_4$ and $C_2H_6$. The total flow rate of the outlet gases was measured using a flow meter (MesaLabs, Definer 220). $C_2H_2$ reaction rate and $C_2H_4$ selectivity was calculated using eq. (2) and eq. (3).

$$C_2H_2 \text{ reaction rate} = \frac{F_{C_2H_2in} - F_{C_2H_2out}}{surface\ area}\ (\text{mol}\cdot\text{min}^{-1}\cdot\text{m}^{-2}) \quad (2)$$

$$C_2H_4 \text{ selectivity} = \frac{F_{C_2H_4out}}{F_{C_2H_2in} - F_{C_2H_2out}} \times 100\ (\%) \quad (3)$$

Where $F_{C_2H_2in}$, $F_{C_2H_2out}$ and $F_{C_2H_2out}$ represent the $C_2H_2$ flow rates at the reactor entrance and $C_2H_2$ and $C_2H_4$ flow rates at outlet, respectively.

To access activation energy, an additional reaction test was carried out in a relatively low temperature range which is suitable to obtain lower $C_2H_2$ conversions (<20%) for calculating the activation energy of the reaction from Arrhenius plot.

### 2.4 DFT calculation

DFT calculations were performed using the first-principles electronic structure calculation program PHASE/0.[21] Self-inconsistent iterations stopped when the convergence energy was less than $2 \times 10^{-6}$ eV. The geometry of the optimized surface and adsorbate-substrate composite was determined by static relaxation. In the structure optimization and transition state calculations, the convergence criterion was set to $2 \times 10^{-6}$ eV for the total energy and $2 \times 10^{-2}$ eV/Å for the force acting on the atoms. In this study, a surface structure containing many local environments is preferable since we investigate the effect of non-equivalent sites on the catalytic properties. In addition, the 1/1 ACs contains a very large number of atoms (184 atoms in Al–Pd–Sc and Ga–Pd–Sc) in the unit cell, resulting in large slab sizes and convergence difficulties on high index surface. For this reason, we prepared the slab models of a (100) surface which contains 7 non-equivalent sites for bulk symmetry as well as all three constituent elements and is a low index surface based on the result of the HAADF structure analysis of Al–Pd–Sc and Ga–Pd–Sc reported by So *et al.*[18,22] (Fig. 1(a)). The slab containing 188 atoms and a vacuum layer of 16 Å. Since the bridge sites were reported to have a smaller $C_2H_2$ adsorption energy than the on-top sites in quasicrystals,[12] the bridge sites were selected as the starting state for adsorption in the present study. Structural stabilization calculations were performed by setting $C_2H_2$ and $C_2H_4$ molecules at 2 Å from the surface on the bridge site between Al, Ga, and Pd on the slab surface (Fig. 1(b)). Calculations were performed by setting $2 \times 2 \times 1$ k-points, and the adsorption energies of $C_2H_2$ ($E_{C_2H_2\ adsorption}$) and $C_2H_4$ ($E_{C_2H_4\ adsorption}$) were evaluated using the equation eq. (4) and eq. (5),

$$E_{C_2H_2\ adsorption} = E_{total} - E_{slab} - E_{C_2H_2} \quad (4)$$

$$E_{C_2H_4\ adsorption} = E_{total} - E_{slab} - E_{C_2H_4} \quad (5)$$

where $E_{total}$ is the total energy of the slab with the absorbed $C_2H_2$ or $C_2H_4$ molecule, $E_{slab}$ is the total energy of the bare slab, and $E_{C_2H_2}$ and $E_{C_2H_4}$ represent the total energy of the isolated $C_2H_2$ and $C_2H_4$ molecules, respectively.

## 3. Results and Discussions

### 3.1 Characterization

Figure 2 presents powder XRD patterns of the $Ga_{55}Pd_{30}Sc_{15}$ and $Al_{55}Pd_{30}Sc_{15}$ 1/1 ACs along with the results of Le Bail fittings[23] obtained by assuming the space groups $Im\bar{3}$ using the Jana 2006 software suite.[24] The red and black lines in the figure represent measured ($I_{obs}$) and calculated ($I_{cal}$) peak intensities, respectively, while the difference between the two and the expected Bragg peak positions are shown by blue line and green vertical bars, respectively. As shown, the experimental peak positions and their intensities are consistent with the calculation confirming high purity of the synthesized 1/1 ACs with the space groups $Im\bar{3}$.

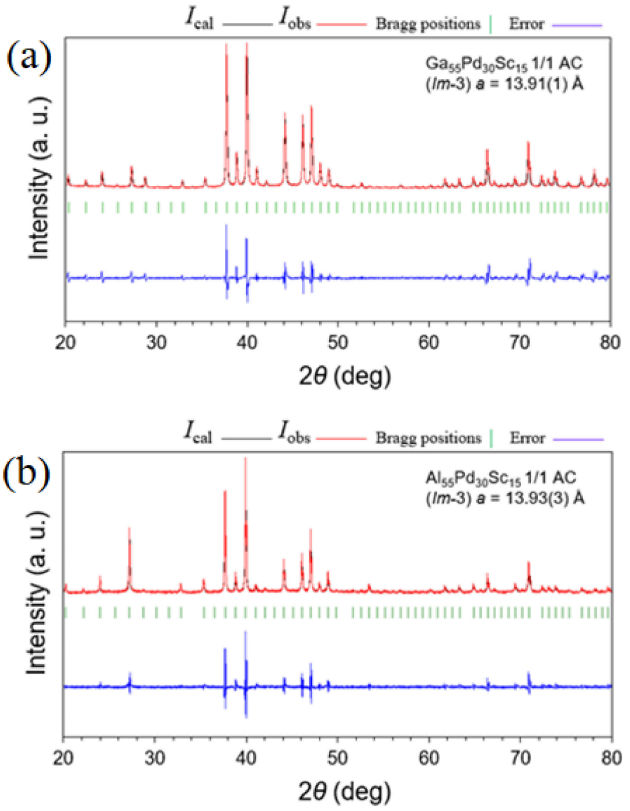


Fig. 2 Le Bail fitting of the powder x-ray diffraction (XRD) patterns of (a) $Ga_{55}Pd_{30}Sc_{15}$ and (b) $Al_{55}Pd_{30}Sc_{15}$ 1/1 ACs. The measured ($I_{obs}$), calculated ($I_{obs}$) peak intensities, the difference between the two and the expected Bragg peak positions are represented by red, black, blue, and green lines, respectively.

The BET specific surface area was low level (0.09–0.11 $m^2 \cdot g^{-1}$) for both samples and the difference were small (Table 1). The crushed surface does not have a high specific surface area, and it can be assumed that a surface similar to that of the bulk is formed macroscopically.

Table 1 BET surface area of prepared catalysts sample. These samples crushed to powder with a particle size of 75 µm or less under argon atmosphere.

| Sample | BET surface area / $m^2 \cdot g^{-1}$ |
|---|---|
| Al-Pd-Sc | 0.09 |
| Ga-Pd-Sc | 0.11 |

### 3.2 Catalytic performance

Figure 3 shows the $C_2H_2$ reaction rate (Fig. 3(a)) and $C_2H_4$ selectivity (Fig. 3(b)) of the Al–Pd–Sc and Ga–Pd–Sc Tsai-type 1/1 ACs for the $C_2H_2$ hydrogenation reaction as a function of the reaction temperature. The reaction rate of Al–Pd–Sc sample increased significantly with over the entire temperature range, whereas that of Ga–Pd–Sc sample gradually increased with temperature. The values of reaction rate of Al–Pd–Sc Sample were much higher than that of Ga–Pd–Sc sample at all the test temperatures. The reaction rate of Al–Pd–Sc sample was $1.63 \times 10^{-3}$ mol·min$^{-1}$·m$^{-2}$ (50.9% in terms of conversion rate) at 200°C, which was approximately 13 times of the corresponding value of Ga–Pd–Sc ($1.09 \times 10^{-6}$ mol·min$^{-1}$). The selectivity was higher than 80% at all temperatures for both samples and the difference between Al–Pd–Sc and Ga–Pd–Sc was small. These results suggest that the elemental substitution of Ga for Al was effective to enhance the catalytic activity and retain a relatively high selectivity even with increased activity.

Figure 4 shows the Arrhenius plot of $C_2H_2$ reaction rate and activation energy of Al–Pd–Sc and Ga–Pd–Sc samples. The activation energy of Al–Pd–Sc sample is estimated as 53.9 kJ/mol, which is lower than that of Ga–Pd–Sc (65.8 kJ/mol). For comparison, the activation energies of several Pd-based catalysts for acetylene hydrogenation reported

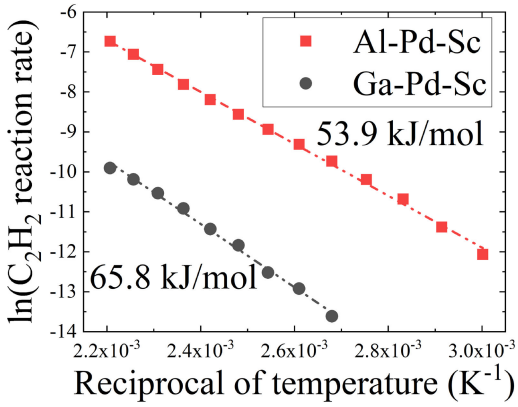


Fig. 4 Arrhenius plot of $C_2H_2$ reaction rate and activation energy of Al–Pd–Sc and Ga–Pd–Sc 1/1 ACs. Approximate straight lines are shown as dotted lines, and activation energies were calculated from the slopes.

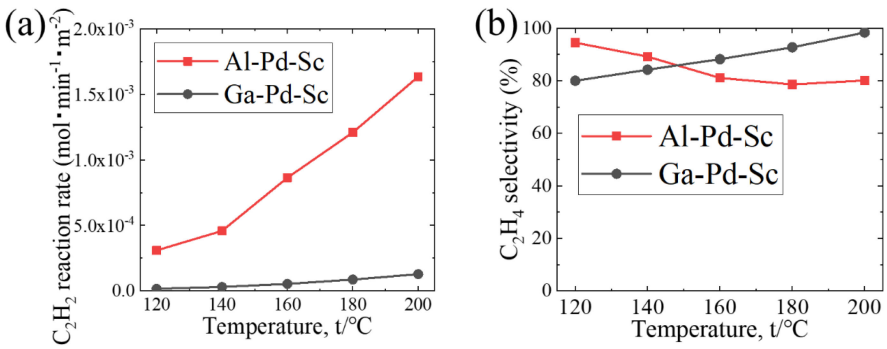


Fig. 3 (a) $C_2H_2$ reaction rate and (b) $C_2H_4$ selectivity of Al–Pd–Sc and Ga–Pd–Sc 1/1 ACs. The feed gas composition of $C_2H_2$, hydrogen, and $N_2$, were 0.5, 5.0, and 23.8 mL/min, respectively.

Table 2 Calculated activation energies from Arrhenius plot of Al–Pd–Sc and Ga–Pd–Sc 1/1ACs and the previously reported values of several Pd-based catalysts.[2,25,26)]

| Catalyst | Sample form | Activation energy E/kJ · mol$^{-1}$ | Reference |
|---|---|---|---|
| Al-Pd-Sc | alloy powder | 53.9 | This study |
| Ga-Pd-Sc | alloy powder | 65.8 | This study |
| Pd | metallic foil | 40.2 | 26 |
| $Pd/SiO_2$ | supported | 42.3 | 25 |
| $CuPd_{0.09}/SiO_2$ | supported | 62.8 | 25 |
| $PdAg/K^+\beta$-zeolite | supported | 59.8 | 2 |

previously were summarized in Table 2.[2,25,26)] The value of activation energy of Al–Pd–Sc 1/1 AC catalyst prepared in this study is smaller than the values of the $CuPd_{0.09}/SiO_2$ and $PdAg/K^+\beta^-$ zeolite catalysts. Compared with $Pd/SiO_2$ and Pd foil catalysts which have been reported to exhibit excellent activity, the activation energy of Al–Pd–Sc was higher. However, these catalysts have poor selectivity,[25,27,28)] whereas Al–Pd–Sc 1/1 AC combines both activity and selectivity to some extent.

### 3.3 DFT calculation

The $C_2H_2$ and $C_2H_4$ adsorption energies of each adsorption sites are shown in Table 3. The $C_2H_2$ adsorption energies of Al–Pd–Sc were lower than that of Ga–Pd–Sc at each site. These results reveal that the adsorption of the reactant acetylene is more likely to occur on the (100) surface of Al–Pd–Sc than on that of Ga–Pd–Sc, which is in good agreement with the experimental results revealing a higher activity of Al–Pd–Sc than that of Ga–Pd–Sc. In addition, the DFT results show that the adsorption energies differed significantly for each adsorption site even when the combination of neighboring atoms was the same. Krajci and Hafner reported that the area around the triangle composed of two atoms of Al or Ga and one atom of Pd is most likely to adsorb $C_2H_2$ in B20 structure Al–Pd and Ga–Pd.[10,11,16)] However, in this study, there was no particular tendency for these sites near this triangle to have small adsorption energies. For example, the adsorption energies at sites 11 and 13 were not small even in the Al–Pd–Sc system.

The structures of the four sites with particularly small adsorption energies (No. 1, No. 5, No. 8, and No. 12) in the final state are shown in Fig. 5 and Fig. 6. The adsorption energies are in decreasing order as No. 8 $\approx$ No. 12 $<$

Table 3 Adsorption energies of $C_2H_2$ and $C_2H_4$ at each site of (100) surface of Al–Pd–Sc and Ga–Pd–Sc.

| Adsorption site | Neighboring atom combination | Adsorption energy E/kJ·mol$^{-1}$ | | | |
|---|---|---|---|---|---|
| | | $C_2H_2$ | | $C_2H_4$ | |
| | | Al-Pd-Sc | Ga-Pd-Sc | Al-Pd-Sc | Ga-Pd-S |
| 1 | Al-Pd, Ga-Pd | -93.8 | 29.1 | -61.1 | -56.5 |
| 2 | Al-Pd, Ga-Pd | 68.7 | 67.5 | -0.1 | 1.8 |
| 3 | Al-Pd, Ga-Pd | -12.3 | 68.6 | 19.5 | 1.5 |
| 4 | Al-Pd, Ga-Pd | -71.6 | 50.5 | -61.5 | -20.8 |
| 5 | Al-Pd, Ga-Pd | -85.2 | -70.7 | -24.4 | -27.6 |
| 6 | Al-Pd, Ga-Pd | -46 | -4.7 | -56.2 | -11.2 |
| 7 | Al-Pd, Ga-Pd | -50.5 | -8.9 | -17.2 | -49 |
| 8 | Al-Pd, Ga-Pd | -97.4 | 8.7 | -22 | -55.7 |
| 9 | Al-Al, Ga-Ga | -81.3 | 67.5 | -1.8 | 1.4 |
| 10 | Pd-Pd | 4.4 | 69.9 | 2.8 | 3.9 |
| 11 | Al-Pd, Ga-Pd | 35.3 | -31.7 | 1.2 | -0.5 |
| 12 | Al-Pd, Ga-Pd | -97.2 | -66.4 | -47.9 | -58.4 |
| 13 | Al-Pd, Ga-Pd | 65.5 | 66.7 | 0.5 | 3.4 |
| 14 | Al-Pd, Ga-Pd | -48.9 | -4.8 | -57.7 | -58.6 |
| 15 | Al-Pd, Ga-Pd | 89.1 | 60.4 | 3.5 | -1.9 |

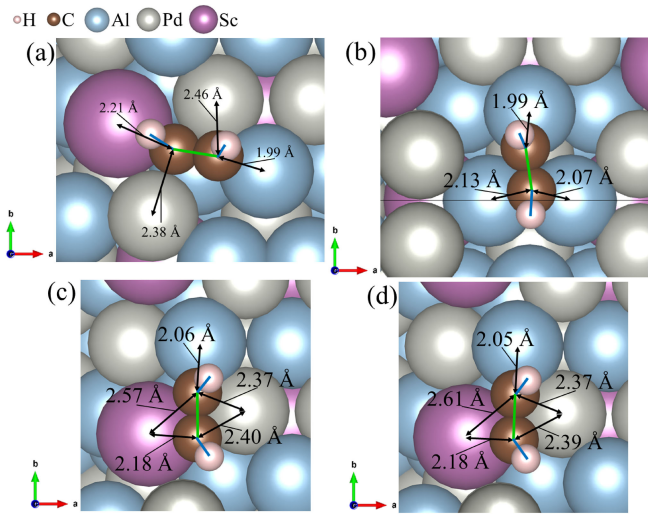


Fig. 5 Top view of Al–Pd–Sc 1/1 AC (100) with adsorbed $C_2H_2$ after structural relaxation started from various initial adsorption sites (a) No. 1, (b) No. 5, (c) No. 8, (d) No. 12. C–C bond and C–H bond were marked with green and blue lines, respectively.

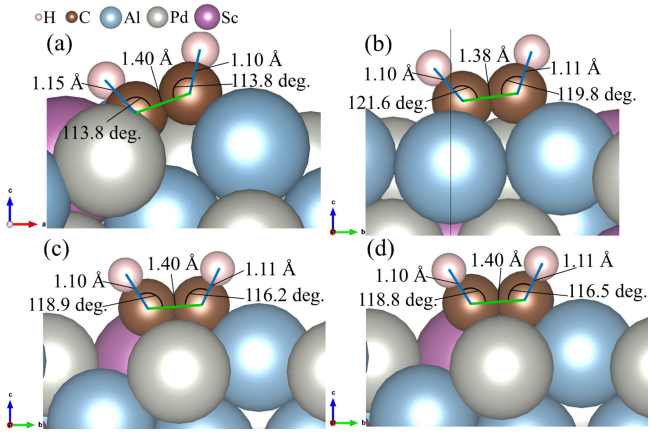


Fig. 6 Side view of Al–Pd–Sc 1/1 AC (100) with adsorbed $C_2H_2$ after structural relaxation started from various initial adsorption sites (a) No. 1, (b) No. 5, (c) No. 8, (d) No. 12. C–C bond and C–H bond were marked with green and blue lines, respectively.

No. 1 < No. 5. The initial sites of No. 8 and No. 12 are almost identical in both adsorption energy and adsorption structure and are considered to have converged to the same final position. In all four initial structures, acetylene was adsorbed on the hollow site in the relaxed structure. Furthermore, three of the sites with the lowest adsorption energies (No. 1, No. 8, and No. 12) adsorbed on the sites adjacent to Sc, suggesting that the sites near Sc may adsorb acetylene more easily. The distance of the C–C bond in the final state was about 1.4 Å for all sites as shown in Fig. 6. This is closer to the double bond length of ethylene (1.34 Å)[29] than the triple bond length of acetylene (1.20 Å).[30] This result suggests that the reactivity differs from site to site in the Tsai type 1/1 ACs as we originally assumed. In both samples, there was a large difference in adsorption energy for each site, but the local structure that causes particularly strong adsorption in the 1/1 ACs is not yet understood. Further calculations of the electron density distribution and the electronic states of the electrons involved in binding are needed to utilize 1/1 AC structure for catalyst design.

In contrast, the adsorption energy of $C_2H_4$ did not differ significantly between Al–Pd–Sc and Ga–Pd–Sc. This result suggests that the desorption rate of $C_2H_4$ on both Al–Pd–Sc and Ga–Pd–Sc samples is close since the adsorption energy of $C_2H_4$ corresponds to the desorption rate of $C_2H_4$. In the $C_2H_2$ hydrogenation reaction, $C_2H_4$ adsorbed on the surface after the reaction undergoes further hydrogenation reaction to form $C_2H_6$, which reduces the selectivity.[31] Al–Pd–Sc exhibited high activity because it easily adsorbs $C_2H_2$, whereas the adsorption energy of $C_2H_4$ did not change obviously with element substitution of Ga by Al. Therefore, $C_2H_4$ was desorbed before the hydrogenation reaction occurred in both Al–Pd–Sc and Ga–Pd–Sc, resulting in Al–Pd–Sc showed high $C_2H_2$ reaction rate and $C_2H_4$ selectivity.

## 4. Conclusion

The catalytic performance in acetylene hydrogenation was investigated for two kinds of Pd-containing Tsai-type 1/1 ACs, Al–Pd–Sc and Ga–Pd–Sc. The Al–Pd–Sc 1/1 AC was found to exhibit a high activity and selectivity in the acetylene hydrogenation reaction. This catalyst shows even higher activity compared to the previously reported Pd-based bimetallic catalyst, suggesting that Tsai-type 1/1 ACs have excellent potential for catalysts.

The DFT calculations of $C_2H_2$ and $C_2H_4$ adsorption energy on (100) surface of Al–Pd–Sc and Ga–Pd–Sc revealed that the Al–Pd–Sc 1/1 AC adsorbs reactant $C_2H_2$ more strongly, while the adsorption of product $C_2H_4$ is comparable to that of the Ga–Pd–Sc 1/1 AC, which is likely responsible for the high activity and selectivity of the Al–Pd–Sc 1/1 AC. In both ACs, large difference in adsorption energy is observed among non-equivalent sites, which suggests superior potential to design catalysts by controlling the local structure at the atomic level using quasicrystals and ACs.

## Acknowledgments

This work supported by New Energy and Industrial Technology Development Organization (NEDO), Japan Society for the Promotion of Science through Grants-in-Aid for Scientific Research (Grants No. JP19H05817, No. JP19H05818) and JST, CREST Grant No. JPMJCR22O3, Japan. The calculations in this study were performed on the Numerical Materials Simulator at NIMS. H. Yoshikawa appreciates the support of the Material Science Human Resource Development Fellowship of Tokyo University of Science.

## REFERENCES

1) I.-C. Oğuz, T. Mineva and H. Guesmi: J. Chem. Phys. **148** (2018) 024701.
2) Y.S. Ma, T. Diemant, J. Bansmann and R.J. Behm: Phys. Chem. Chem. Phys. **13** (2011) 10741–10754.
3) D.J. Gorin, B.D. Sherry and F.D. Toste: Chem. Rev. **108** (2008) 3351–3378.
4) J.R. Kitchin, J.K. Nørskov, M.A. Barteau and J.G. Chen: Phys. Rev. Lett. **93** (2004) 156801.

5) S. Takeuchi, K. Edagawa, A.P. Tsai and K. Kimura: *Physics of Quasicrystals*, (Asakura-Syoten, Tokyo, 2012) pp. 30–68.
6) A.P. Tsai and A. Yamamoto: Philos. Mag. **87** (2007) 2599–2600.
7) K. Abe, R. Tsukuda, N. Fujita and S. Kameoka: RSC Adv. **11** (2021) 15296–15300.
8) M. Krajčí and J. Hafner: ChemCatChem **8** (2016) 34–48.
9) M. Krajčí, A.-P. Tsai and J. Hafner: J. Catal. **330** (2015) 6–18.
10) M. Krajčí and J. Hafner: J. Phys. Chem. C **116** (2012) 6307–6319.
11) M. Krajčí and J. Hafner: J. Catal. **295** (2012) 70–80.
12) M. Krajčí and J. Hafner: J. Catal. **278** (2011) 200–207.
13) M. Krajčí and J. Hafner: Phys. Rev. B **84** (2011) 115410.
14) M. Yoshimura and A.P. Tsai: J. Alloy. Compd. **342** (2002) 451–454.
15) A.P. Tsai and M. Yoshimura: Appl. Catal. A Gen. **214** (2001) 237–241.
16) M. Krajčí and J. Hafner: Phys. Rev. B **87** (2013) 035436.
17) A.-P. Tsai: J. Non-Cryst. Solids **334–335** (2004) 317–322.
18) Y.G. So, A. Katagiri, R. Tamura and K. Edagawa: Philos. Mag. Lett. **98** (2018) 292–300.
19) Y.G. So and K. Edagawa: Mater. Trans. **50** (2009) 948–951.
20) A.J. McCue, C.J. McRitchie, A.M. Shepherd and J.A. Anderson: J. Catal. **319** (2014) 127–135.
21) T. Yamasaki, A. Kuroda, T. Kato, J. Nara, J. Koga, T. Uda, K. Minami and T. Ohno: Comput. Phys. Commun. **244** (2019) 264–276.
22) Y.G. So, M. Nagao, T. Nagai and K. Kimoto: J. Alloy. Compd. **543** (2012) 7–11.
23) A. Le Bail, H. Duroy and J.L. Fourquet: Mater. Res. Bull. **23** (1988) 447–452.
24) V. Petříček, M. Dušek and L. Palatinus: Z. Krist.-Cryst. Mater. **229** (2014) 345–352.
25) M.R. Ball, K.R. Rivera-Dones, E.B. Gilcher, S.F. Ausman, C.W. Hullfish, E.A. Lebron and J.A. Dumesic: ACS Catal. **10** (2020) 8567–8581.
26) H. Molero, B.F. Bartlett and W.T. Tysoe: J. Catal. **181** (1999) 49–56.
27) J. Osswald, K. Kovnir, M. Armbruster, R. Giedigleit, R.E. Jentoft, U. Wild, Y. Grin and R. Schlogl: J. Catal. **258** (2008) 219–227.
28) J. Osswald, R. Giedigkeit, R.E. Jentoft, M. Armbruster, F. Girgsdies, K. Kovnir, T. Ressler, Y. Grin and R. Schlogl: J. Catal. **258** (2008) 210–218.
29) W. Majer, P. Lutzman and W. Hüttner: Mol. Phys. **83** (1994) 567–578.
30) D.J. Gearhart, J.F. Harrison and K.L.C. Hunt: Int. J. Quantum Chem. **95** (2003) 697–705.
31) D.H. Mei, M. Neurock and C.M. Smith: J. Catal. **268** (2009) 181–195.